Plasmonics (2020) 15:1959–1966
https://doi.org/10.1007/s11468-020-01225-4

The Effect of Annealing Temperature on the Plasma Edge in Reflectance Spectra of Al/Al_2O_3 Composites Synthesized by Thermal Oxidation of Aluminum Thin Films

Kamal Kayed [1] · **Lubna Alberni** [1]

Received: 19 April 2020 / Accepted: 29 June 2020 / Published online: 3 July 2020
© Springer Science+Business Media, LLC, part of Springer Nature 2020

Abstract

In this study, the structural and optical properties of aluminum oxide thin films were investigated. Aluminum oxide thin films were prepared on silicon and glass substrate by DC magnetron sputtering of aluminum targets with subsequent thermal oxidation of the aluminum-deposited thin films. Important result obtained included the presence of a plasma edge for the individual aluminum atoms. In addition, the temperatures that resulted in the highest concentration of surface plasmons were determined. On other hand, the relationship between the plasma edge and the optical energy gap was investigated.

Keywords Silver oxide · Thin film · DC magnetron sputtering · Annealing · Plasmon · Plasma edge

Introduction

Silver oxide thin films gained the attention of many research groups in recent years [1–13], mainly because they exhibit significant applications in gas sensors, passivation, organic field-effect transistors, perovskite solar cells, organic light-emitting diode encapsulation, optical data storage, and surface plasmon optics, etc.

There are numerous deposition techniques for obtaining Al_2O_3 thin films as thermal evaporation [2],atomic layer deposition (ALD) [13–15], magnetron sputtering [16, 17], pulsed-laser deposition (PLD) [18], spray pyrolysis [19, 20], and sol-gel coating [21].

Valence electrons in any conductor act like free electrons, where the collision among the electrons is similar among gas molecules that are described in the kinetic theory of gases [22]. Optical properties of metals are produced due to the interaction between the fallen photons on the surface and the electronic cloud [22]. Optical reflectivity is considered the most important physical property of the metal layers, which generally relates to the interaction between the light and the free electrons which could be expressed by the equation of dispersion as follows [22, 23]:

$$\omega_{\mathrm{p}} = \sqrt{\frac{4\pi N e^2}{\varepsilon_\infty m^*}} \quad (1)$$

where N is the concentration of conducting electrons, e the electron charge, $_\infty$ the high frequency (visible wavelength), ε the dielectric constant, and m^* the electron effective mass.

Both electron concentration and electron effective mass affect this plasma edge [22] and could be directly determined from the reflecting spectra where dramatic change of reflectivity happens at the plasma edge as a result of photon reflection from the conduction band electron plasma oscillations [23]. Furthermore, equation indicates that, when carrier concentration and hence typically the conductivity are increased, the plasma edge moves to high frequencies (shorter wavelengths) [23]. In this paper, we are interested in identifying the factors affecting the plasma edge formed in the reflectance spectra of aluminum oxide thin films prepared by the thermal oxidation of the aluminum thin films deposited by DC magnetron sputtering of aluminum targets.

Experimental

Sample Preparation

Pure Al thin films (99.99%) were deposited at room temperature onto thoroughly cleaned n-type Si (100) and glass substrates from a high-purity Al (99.99%) target using DC

✉ Kamal Kayed
khmk2000@gmail.com

[1] Department of physics, Faculty of Science, Damascus University, Damascus, Syria

Table 1 The thermal treatment conditions for each sample

Deposition parameters	
Argon flow rate	5.2 sccm
Sputtering power	100 W
Work pressure	4.3×10^{-3} Torr
Vacuum pressure	8.8×10^{-5} Torr
Substrate-target distance	7 cm
The duration of the deposition process	7 min

Table 2 The thermal treatment conditions for each sample

Sample code	Temperature (°C)	Thermal processing time (h)
A	100	1
B	200	1
C	300	1
D	400	1
E	500	1
F	500	2

magnetron sputtering process. The substrate placed below the source in the direction of ablated material flux. The deposition conditions are given in Table 1.

Each deposited film was annealed in air at specific temperature (100, 200, 300, 400, and 500 °C) in order to oxidize the aluminum atoms. Table 2 contains the thermal treatment conditions for each sample.

Sample Characterization

Crystallite structure of the films was measured by X-ray diffraction (XRD) using (Stoe StadiP) transmission X-ray diffractometer employing a Cu-Kα_1 ($\lambda = 1.54060$ Å) source. The optical transmittance and reflection spectra were recorded with a UV–Vis spectrophotometer (Cary 5000).

Results and Discussion

X-ray diffraction measurements were carried out on the aluminum oxide thin films. The XRD profiles of these samples are shown in Fig. 1. As seen in this figure, the A sample spectrum contains a large number of peaks and broad bands, some of which are related to aluminum metal and the rest are

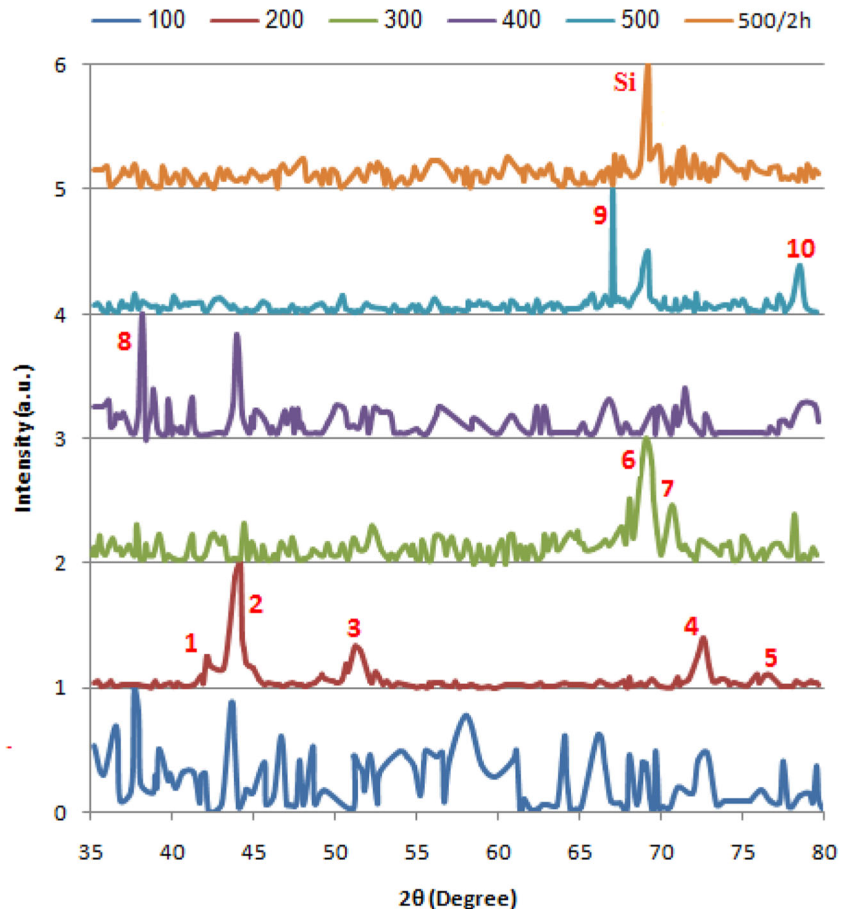

Fig. 1 The XRD spectra of the prepared samples

Table 3 The main features of all the peaks observed in XRD spectra

Peak number	Peak position	Chemical formula	Crystal structure	Crystalline plane	CSM card No	Samples
1	44.15°	Al_2O_3	Rhombohedra	300	1-1243	A, B
2	44.01°	Al_2O_3	Rhombohedra	113	1-1243	A, B, D
3	51.22°	Al_2O_3	Kappa	–	8-13	A, B, F
4	72.57°	Al_2O_3	Kappa	–	8-13	A, B, C, D
5	76.73°	Al	FCC	311	89-2769	B
6	69.16°	Al_2O_3	Alpha	–	1-1296	A, C, E, F
7	70.68°	Al_2O_3	Kappa	–	8-13	C, D
8	38.33°	Al	FCC	111	89-2769	A, C, D
9	67.03°	Al_2O_3	FCC	440	77-0396	D, E, F
10	78.47°	Al	FCC	222	89-2837	A, B, C, D, E, F

related to some phases of aluminum oxide (alpha, beta, kappa, gamma). This great diversity of phases makes it difficult to make an accurate description of the structural composition of this sample. On the other hand, when the annealing temperature increases, the number of peaks becomes limited and the spectrum becomes clearer. Therefore, we determined the main peaks in the spectra of samples from B to F. Table 3 contains the main features of all the peaks observed in XRD spectra. We have taken into account the determination of the samples in which each of the main peak clearly shows. It can be seen that the alpha phase peak appears in the spectra of the C, E, and F samples. In addition, the samples that have a high percentage of aluminum metal are A, D, and E. The rhombohedra phase of aluminum oxide has a high percentage in three samples (A, B, and D). It is interesting to note that the peak of the silicon does not show in the spectra of the samples except for the sample (F) spectrum, which indicates the low density of this sample and that it has a porous structure.

The structures we obtained are more diversified than that recorded in previous work [2], which adopted the method of thermal evaporation to obtain aluminum thin films.

The ratio of non-oxidizing aluminum atoms in each sample can be used to investigate the stability of the bonds (Al–O) during thermal treatment. This ratio is proportional to the sum of the relative areas of the aluminum peaks in the XRD spectrum. In order to calculate the relative areas, a fitting process performed for each peak adoption of the Gaussian and Lorentzian shape. Table 4 contains the position and the area of each peak, in addition to the total area (S_{Al}%) of the prepared samples.

Table 4 The position, the area of each peak, and the total area (S_{Al}%) of the prepared samples

Peak position⇨	44.4°	38.3°	64.8°	78.2°	
Sample	S_1%	S_2%	S_3%	S_4%	S_{Al}%
A	4.30	19.00	1.00	4.8	29.10
B	17.50	–	–	–	17.50
C	0.05	–	–	0.06	0.11
D	5.10	–	–	8.32	13.42
E	7.04	–	–	–	7.04
F	0.38	–	–	1.11	1.49

Figure 2 illustrates the total area (S_{Al}%) as a function of annealing temperature.

It can be observed that in general, the ratio of aluminum atoms decreases with increasing annealing temperature except for the sample D (400 °C), where the ratio of non-oxidizing aluminum atoms increases. This indicates that oxidation processes are limited at the temperature 400 °C where a low-concentration mixture of the rhombohedra and cubic Al_2O_3 phases is formed. On the other hand, the annealing at 300 °C (sample C) appears to be suitable for the formation of the phase alpha and kappa p with high oxidation rates. Almost complete oxidation process also occurs in the case of the sample F (500 °C/2 h) where the alpha stable phase predominates.

Figure 3 shows the reflectance spectra of the prepared samples.

By comparing this figure with Fig. 2, we notice that the effect of annealing temperature on reflectance is not the same as its effect on the proportion of aluminum in the film, and this makes us believe that the reflectivity is not related to the ratio of aluminum atoms. On the other hand, we note that in all spectra, there is a wide band to the left of the plasma edge and that this band slopes sharply toward the plasma edge, and we note that the length of the slope decreases with both the increase in annealing temperature and in the reflectance. This can be attributed to the different optical behavior on both sides of the plasma edge. In the case where $\lambda < \lambda_p$, light interacts with individual aluminum nanoparticles. In the case where $\lambda > \lambda_p$, light interacts with surface plasmons of larger Al nanoparticles, where, the concentration of surface plasmons depends on the annealing temperature, and accordingly, we

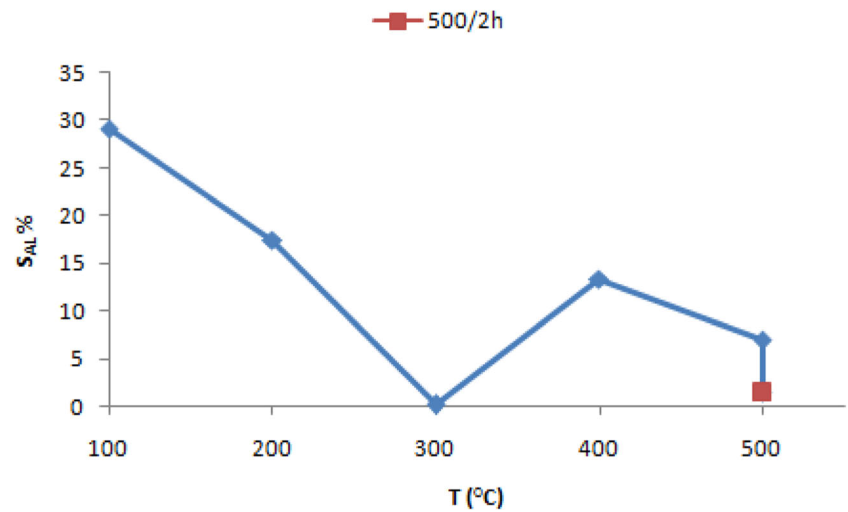

Fig. 2 S_{Al}% as a function of annealing temperature

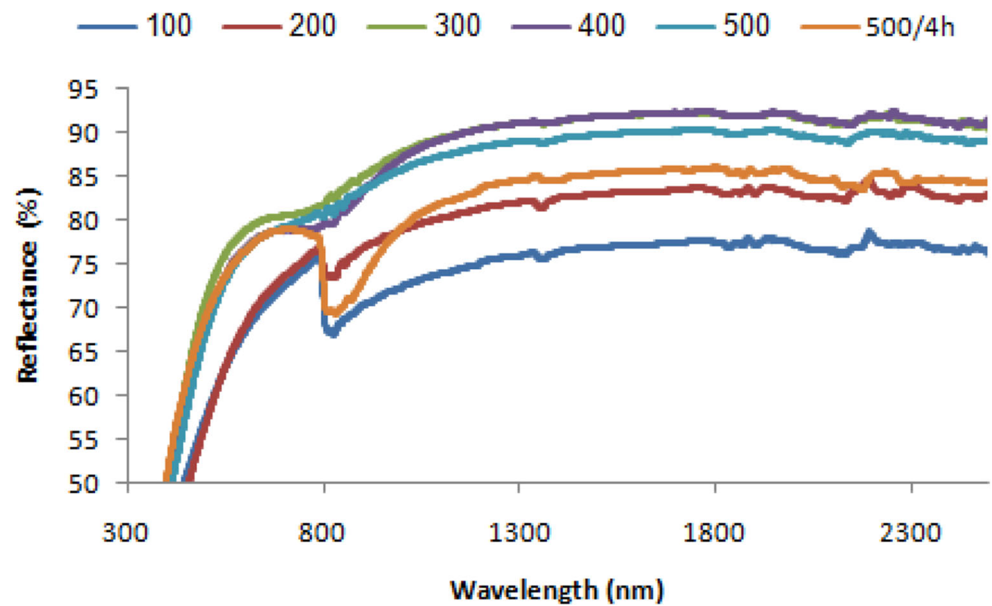

Fig. 3 The reflectance spectra of the prepared samples

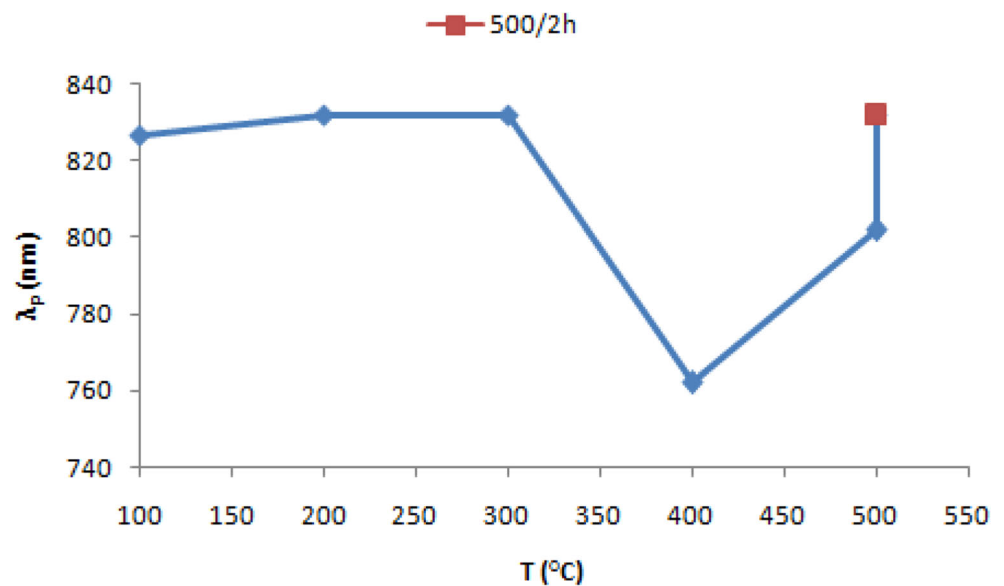

Fig. 4 Plasma edge as a function of annealing temperature

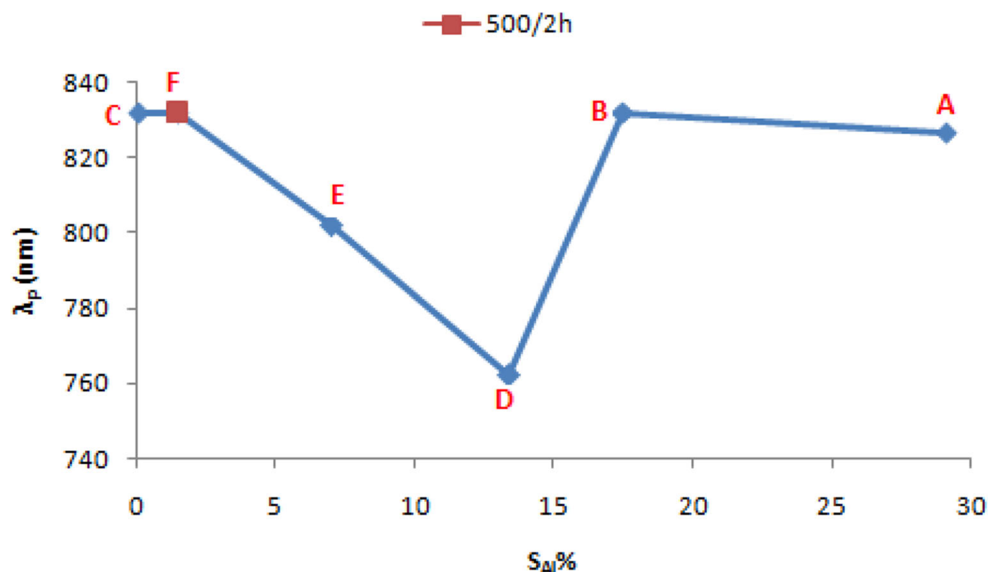

Fig. 5 Plasma edge as a function of the total area (S_{Al}%)

can conclude from Fig. 3 that samples C, E, and D have largest Al nanoparticles compared to the rest of the samples.

The presence of two types of aluminum nanostructures leads to an important conclusion, which is the presence of a plasma edge for individual aluminum atoms (λ'_p). Depending on Fig. 3, it can be expected that this edge is in the ultraviolet range ($\lambda'_p < 300$ nm).

As mentioned in the introduction, samples with plasma edges with short wavelengths have high concentration of charge carriers. By applying this rule to the Fig. 4 that illustrates plasma edge as a function of annealing temperature, we conclude that sample D has the highest concentration of charge carriers followed by sample E. The charge carriers here are intended to be aluminum surface plasmons.

Figure 5 shows plasma edge as a function of the total area (S_{Al}%). We notice that C and F samples are on the left side of the figure and have high plasma edges because of their low concentrations of surface plasmons.

The A and B samples, which are located on the right side of the shape, also have high plasma edges despite having high concentrations of aluminum metal. This is due to the fact that the high concentration of metal particles and their interaction with each other prevents the occurrence of response vibrations of surface plasmons. We conclude from the above that the samples D and E are best suited as Al/Al_2O_3 composites for surface plasmon applications because they have high concentrations of surface plasmons.

Because the prepared films were opaque, we calculated the optical energy band gap from the reflectance spectra using

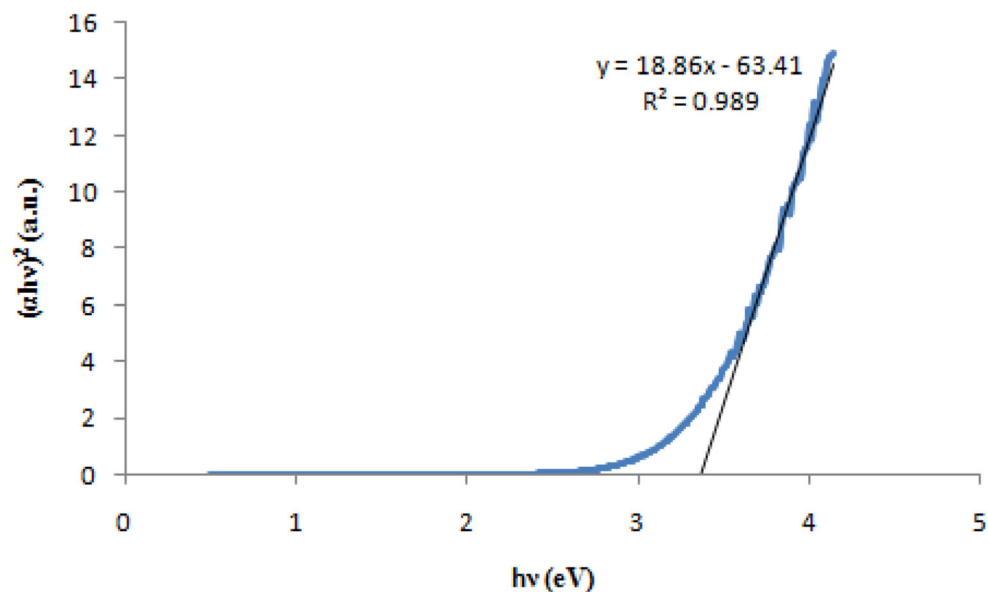

Fig. 6 Variation of $(\alpha h\ )^2$ against h for sample E

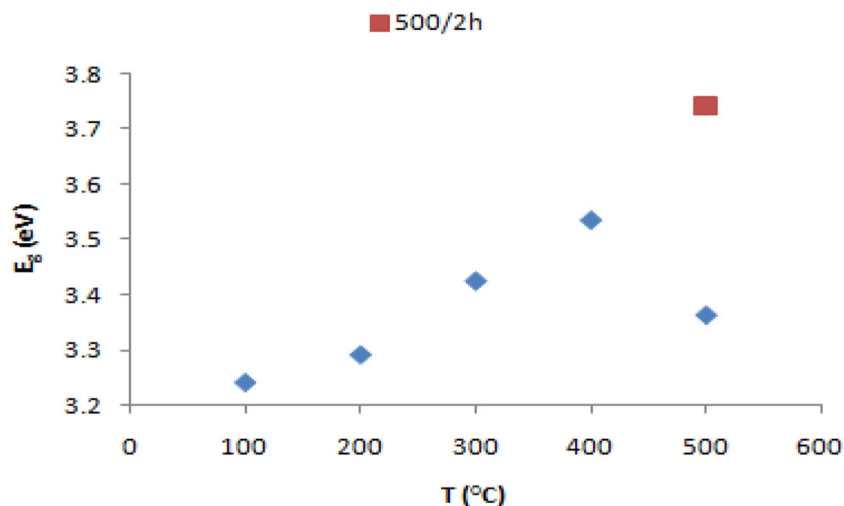

Fig. 7 The optical band gap as a function of annealing temperature

Kubelka-Munk method [24, 25]. Figure 6 shows the method of calculating the energy band gap in the case of sample E.

Figure 7 shows the optical band gap as a function of annealing temperature. We notice that the band gap increases with increasing annealing temperature, but at the temperature of 400 °C (sample D), the band gap decreases. However, it increases again with doubling the treatment time using the same temperature.

This behavior can be understood by investigating the relationship between the optical energy band gap and the plasma edge (Fig. 8).

We notice that, for $\lambda_p < 830$ nm, the band gap decreases when the plasma edge increases. For higher plasma edges, the band gap becomes independent of the plasma edge, in which case the band gap related only to the structural composition of the thin film. The great effect of the ratio of the non-oxidizing aluminum atoms appears here, as the A and B samples have low values for the band gap because they have a high content of the non-oxidized aluminum atoms. Figure 8 is very important because it helps to precisely determine the state at which the plasma effect begins to appear.

We found that, in the samples A, C, E, and F, the band gap related only to the structural composition of the thin film. This also appears applicable to the plasma edge. Despite the many phases formed in these samples, it appears that the plasma edge is proportional to the concentration of the alpha phase. The formation of this phase is associated with high oxidation rates; this is the reason for obtaining a small concentration of aluminum in the sample F, which leads to a low concentration of surface plasmons, and it will naturally increase the film's dielectric constant. In addition, the significant effect of the grain size on the surface plasmon resonance [26] must be taken into account.

Finally, the optical measurement of the plasma frequency is seen as a non-contact probe to measure the electrical properties [23]. In our case, this seems to be incorrect for all cases,

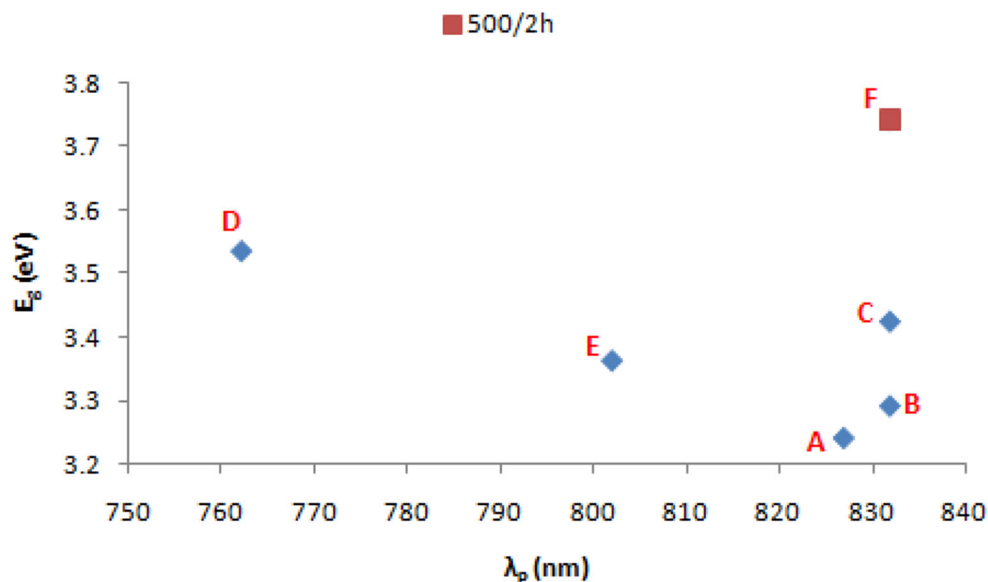

Fig. 8 The optical band gap as a function of plasma edge

especially for $\lambda_p < 300$ nm, as the band gap (which can be expressed as a measure of conductivity) decreases with increasing the plasma edge. The diversity of structural phases, along with the diversity of preparation conditions (annealing temperature), is the main factor determining the overall optical and electrical characteristics of the prepared thin films. However, investigating the relationship between the optical band gap and the plasma edge appears necessary for the engineering design of Al/Al_2O_3 composites, which make them suitable for specific applications.

Conclusions

In this work, aluminum oxide films are deposited by DC magnetron sputtering of aluminum metal on silicon and glass substrates with subsequent oxidation of deposition products at different annealing temperatures. Annealing processes were performed in the air using an oven. The effect of temperature on XRD and reflectance spectra of the prepared films was studied. The results obtained included the following:

- The structural composition of the prepared films is highly dependent on the annealing temperature.
- The annealing at 500 °C for 2 h provides almost complete oxidation with a high alpha stable phase ratio.
- In addition to the plasma threshold (λ_p) caused by aluminum nanoparticles, we monitored the presence of a plasma edge for the individual aluminum atoms (λ'_p).
- The annealing temperatures in the range 400–500 °C are best suited as Al/Al_2O_3 composites for surface plasmon applications because they have high concentrations of surface plasmons.
- The curve E_g vs. λ_p is very important for the engineering design of Al/Al_2O_3 composites for surface plasmon applications.

Acknowledgments The authors would like to thank the Syrian Atomic Energy Commission and the University of Damascus for providing the facility to carry out this research. They would also like to thank Dr. B. Abdallah for the assistance during working on the DC magnetron sputtering system.

References

1. Lei D, Yu X, Song L, Gu X, Li G, Yang D (2011) Modulation of atomic-layer-deposited Al_2O_3 film passivation of silicon surface by rapid thermal processing. Appl Phys Lett 99:5–8
2. Boratto MH, Scalvi LVA (2014) Deposition ofAl_2O_3 by resistive evaporation and thermal oxidation of Al to be applied as a transparent FET insulating layer. Ceram Int 40:3785–3791
3. Mohammadi MR (2014) Semiconductor TiO_2-Al_2O_3 thin film gas sensors derived from aqueous particulate sol-gel process. Mater Sci Semicond Process 27:711–718
4. Liang Z, Bi Z, Gao K, Fu Y, Guan P, Feng X, Chai Z, Xu G, Xu X (2019) Interface modification via Al 2 O 3 with retarded charge recombinations for mesoscopic perovskite solar cells fabricated with spray deposition process in the air. Appl Surf Sci 463:939–946
5. Baek Y, Lim S, Kim LH, Park S, Lee SW, Oh TH, Kim SH, Park CE (2016) Al_2O_3/TiO_2 nanolaminate gate dielectric films with enhanced electrical performances for organic field-effect transistors. Organic Electronics 28:139–146
6. Han YC, Kim E, Kim W, Im HG, Bae BS, Choi KC (2013) A flexible moisture barrier comprised of a SiO_2-embedded organic-inorganic hybrid nanocomposite and Al_2O_3 for thin-film encapsulation of OLEDs. Organic Electronics 14:1435–1440
7. Ding X, Zhang J, Zhang H, Ding H, Huang C, Li J, Shi W, Jiang X, Zhang Z (2014) ZrO2 insulator modified by a thin Al_2O_3 film to enhance the performance of InGaZnO thin-film transistor. Microelectron Reliab 54:2401–2405
8. Takhar K, Upadhyay BB, Yadav YK, Ganguly S, Saha D (2019) Al_2O_3 formed by post plasma oxidation of Al as a gate dielectric for AlGaN/GaN MIS-HEMTs. Appl Surf Sci 481:219–225
9. Kayed K (2017) An innovative method for measuring the optical band gap of oxidized surface layer of aluminum tablets based on absorption spectra. IJNeaM 11:71–76
10. Meza-Arroyo J, Syamala Rao MG, Mejia I, Quevedo-López MA, Ramírez-Bon R (2019) Low temperature processing of Al_2O_3-GPTMS-PMMA hybrid films with applications to high-performance ZnO thin-film transistors. Appl Surf Sci 467–468: 456–461
11. Song X, Xu J, Liu L, Lai PT, Tang WM (2019) Improved interfacial and electrical properties of few-layered MoS 2 FETs with plasma-treated Al_2O_3 as gate dielectric. Appl Surf Sci 481:1028–1034
12. Koda Y, Sugita H, Suwa T, Kuroda R, Goto T, Teramoto A, Sugawa S (2016) Low leakage current Al_2O_3 metal-insulator-metal capacitors formed by atomic layer deposition at optimized process temperature and O_2 post deposition annealing. ECS Trans 72:91–100
13. Yota J, Shen H, Ramanathan R (2013) Characterization of atomic layer deposition HfO_2, Al_2O_3, and plasma-enhanced chemical vapor deposition Si3N4as metal–insulator–metal capacitor dielectric for GaAs HBT technology. J Vac Sci Technol A 31(1):01A134
14. Kwak HY, Kwon HM, Jung YJ, Kwon SK, Jang JH, Il Choi W, Ha ML, Il Lee J, Lee SJ, Lee HD (2013) Characterization of Al_2O_3-HfO_2-Al $_2O_3$ sandwiched MIM capacitor under DC and AC stresses. Solid State Electron 79:218–222
15. Gakis GP, Vahlas C, Vergnes H, Dourdain S, Tison Y, Martinez H, Bour J, Ruch D, Boudouvis AG, Caussat B, Scheid E (2019) Investigation of the initial deposition steps and the interfacial layer of atomic layer deposited (ALD) Al_2O_3 on Si. Appl Surf Sci 492: 245–254
16. Murray J, Huebner W, O'Keefe MJ, Wilder K, Eatinger R, Kuhn W, Krueger DS, Wolf JA (2011) Sputter deposition of thin film MIM capacitors on LTCC substrates for RF bypass and filtering applications. IMAPS'03 2011:000747–000752
17. Mao S, Yang H, Huang F, Xie T, Song Z (2011) Corrosion behaviour of sintered NdFeB coated with Al/Al_2O_3 multilayers by magnetron sputtering. Appl Surf Sci 257:3980–3984
18. Ben Rabha M, Salem M, El Khakani MA, Bessais B, Gaidi M (2013) Monocrystalline silicon surface passivation by Al_2O_3/porous silicon combined treatment. MSEB 178:695–697
19. Adamopoulos G, Thomas S, Bradley DDC, McLachlan MA, Anthopoulos TD (2011) Low-voltage ZnO thin-film transistors based on Y_2O_3 and Al_2O_3 high-k dielectrics deposited by spray pyrolysis in air. Appl Phys Lett 98:98–101
20. Dhonge BP, Mathews T, Sundari ST, Thinaharan C, Kamruddin M, Dash S, Tyagi AK (2011) Spray pyrolytic deposition of transparent aluminum oxide (Al_2O_3) films. Appl Surf Sci 258:1091–1096.040

21. Nayak PK, Hedhili MN, Cha D, Alshareef HN (2013) High performance In_2O_3 thin film transistors using chemically derived aluminum oxide dielectric. Appl Phys Lett 103:1–5
22. Born M, Wolf E (2005) Principles of optics, 6th edn. Cambridge University Press, Cambridge
23. Perkins JD, Teplin CW, van Hest MFAM, Alleman JL, Li X, Dabney MS, Keyes BM, Gedvilas LM, Ginley DS, Lin Y, Lu Y (2004) Optical analysis of thin film combinatorial libraries. Appl Surf Sci 223:124–132
24. Kubelka P, Munk F (1931) Ein beitrag zur optik der farbanstriche. Z Tech Phys 12:593–601
25. Kubelka P (1948) New contributions to the optics of intensely light-scattering materials. Part I. J Opt Soc Am 38:448–457
26. Kayed K (2020) The optical properties of individual silver nanoparticles in Ag/Ag_2O composites synthesized by oxygen plasma treatment of silver thin films. Plasmonics. https://doi.org/10.1007/s11468-020-01169-9

Publisher's Note Springer Nature remains neutral with regard to jurisdictional claims in published maps and institutional affiliations.